

One-step synthesis of $ThMn_{12}$-type $Sm_{0.8}Zr_{0.2}Fe_{11}SiB_x$ (x=0-0.2) ribbon magnets via rapid solidification

Chi Zhang(张驰), Hui-Dong Qian(千辉东), Wenyun Yang(杨文云), Jingzhi Han(韩景智), Xuegang Chen(陈学刚), Jinbo Yang(杨金波)

Citation: Chin. Phys. B, 2025, 34 (**7**): 077501. DOI: 10.1088/1674-1056/add006
http://cpb.iphy.ac.cn; http://iopscience.iop.org/cpb

What follows is a list of articles you may be interested in

Phase structure evolution and coercivity mechanism of high-Co containing permanent magnets

Min Huang(黄敏), Yong Ding(丁勇), Zhihe Zhao(赵之赫), Chunguo Wang(王春国), Bo Zhou(周波), Lei Liu(刘雷), Yingli Sun(孙颖莉), and Aru Yan(闫阿儒)

Chin. Phys. B, 2024, 33 (**11**): 117503. DOI: 10.1088/1674-1056/ad6b82

Impact of Co^{2+} substitution on structure and magnetic properties of M-type strontium ferrite with different Fe/Sr ratios

Yang Sun(孙洋), Ruoshui Liu(刘若水), Huayang Gong(宫华扬), and Baogen Shen(沈保根)

Chin. Phys. B, 2024, 33 (**10**): 107506. DOI: 10.1088/1674-1056/ad6554

Phase structure evolution and its effect on magnetic and mechanical properties of B-doped Sm_2Co_{17}-type magnets with high Fe content

Yao-Wen Li(李耀文), Zhuang Liu(刘壮), Hai-Chen Wu(吴海辰), Fang Wang(王芳), Chao-Qun Zhu(竺超群), Dong-Liang Tan(谭栋梁), Yu Liu(刘宇), Yang Yang(羊杨), Ming-Xiao Zhang(张明晓), Ren-Jie Chen(陈仁杰), and A-Ru Yan(闫阿儒)

Chin. Phys. B, 2024, 33 (**9**): 097504. DOI: 10.1088/1674-1056/ad5535

Preparation and magnetic hardening of low Ti content $(Sm,Zr)(Fe,Co,Ti)_{12}$ magnets by rapid solidification non-equilibrium method

Xing-Feng Zhang(张兴凤), Li-Bin Liu(刘立斌), Yu-Qing Li(李玉卿), Dong-Tao Zhang(张东涛), Wei-Qiang Liu(刘卫强), and Ming Yue(岳明)

Chin. Phys. B, 2024, 33 (**9**): 097503. DOI: 10.1088/1674-1056/ad58c4

Effect of In doping on the evolution of microstructure, magnetic properties and corrosion resistance of NdFeB magnets

Yuhao Li(李豫豪), Xiaodong Fan(范晓东), Zhi Jia(贾智), Lu Fan(范璐), Guangfei Ding(丁广飞), Xincai Liu(刘新才), Shuai Guo(郭帅), Bo Zheng(郑波), Shuai Cao(曹帅), Renjie Chen(陈仁杰), and Aru Yan(闫阿儒)

Chin. Phys. B, 2024, 33 (**3**): 037508. DOI: 10.1088/1674-1056/ad0e5c

---

One-step synthesis of $ThMn_{12}$-type $Sm_{0.8}Zr_{0.2}Fe_{11}SiB_x$ (x =0–0.2) ribbon magnets via rapid solidification

Chi Zhang(张驰)[1], Hui-Dong Qian(千辉东)[2†], Wenyun Yang(杨文云)[2], Jingzhi Han(韩景智)[2], Xuegang Chen(陈学刚)[1,3,‡], and Jinbo Yang(杨金波)[2,4,5,6,§]

[1] *Center of Free Electron Laser & High Magnetic Field, Leibniz International Joint Research Center of Materials Sciences of Anhui Province, Institutes of Physical Science and Information Technology, Anhui University, Hefei* 230601, *China*

[2] *Institute of Condensed Matter and Material Physics, School of Physics, Peking University, Beijing* 100871, *China*

[3] *Information Materials and Intelligent Sensing Laboratory of Anhui Province, and Anhui Provincial Key Laboratory of Magnetic Functional Materials and Devices, Anhui University, Hefei* 230601, *China*

[4] *State Key Laboratory for Mesoscopic Physics and School of Physics, Peking University, Beijing* 100871, *China*

[5] *Beijing Key Laboratory for Magnetoelectric Materials and Devices, Beijing* 100871, *China*

[6] *Peking University Yangtze Delta Institute of Optoelectronics, Beijing* 100871, *China*

(Received 13 January 2025; revised manuscript received 8 April 2025; accepted manuscript online 24 April 2025)

$ThMn_{12}$-type iron-rich rare-earth permanent magnetic materials have garnered significant attention due to their exceptional intrinsic magnetic properties. However, challenges such as the metastable nature of the $ThMn_{12}$-type phase, excessively small single-domain grain size, and complex fabrication processes have hindered the achievement of high phase purity, uniform microstructure, and desirable extrinsic performance. In this study, we directly synthesized $ThMn_{12}$-type $Sm_{0.8}Zr_{0.2}Fe_{11}SiB_x$ (x = 0–0.2) ribbon magnets via boron doping combined with a one-step rapid solidification method. This approach not only simplifies the fabrication process but also enhances phase stability and achieves a uniform microstructure with high $ThMn_{12}$-type phase purity. By optimizing the boron content and cooling rate, the resulting magnets exhibit a coercivity (H_c) of 6222 Oe, a remanence (M_r) of 80 emu/g, and a remanence ratio (M_r/M_s) of 0.71. This work demonstrates a streamlined approach to producing high-performance $ThMn_{12}$-type magnets and provides insights into their practical application potential.

Keywords: $ThMn_{12}$-type, permanent magnet, rapid solidification, phase stabilization, microstructure

PACS: 75.50.Ww, 75.75.–C, 75.75.Cd

DOI: 10.1088/1674-1056/add006 **CSTR:** 32038.14.CPB.add006

1. Introduction

Permanent magnetic materials are indispensable in a wide range of applications, including electric motors, generators, and magnetic storage devices.[1–3] The development of high-performance magnets with enhanced intrinsic and extrinsic properties is a persistent challenge in materials science, particularly for iron-rich rare-earth magnets, which have garnered significant interest due to their potential to offer superior magnetic properties.[4–9] Among these, $ThMn_{12}$-type rare-earth permanent magnets have emerged as a promising candidate because of their excellent intrinsic magnetic properties, including high magnetization and high anisotropy field.[10–13] These characteristics make $ThMn_{12}$-type magnets an attractive alternative to traditional NdFeB and SmCo magnets, particularly due to their cost-effectiveness and environment-friendly properties.[9,14,15]

$ThMn_{12}$-type magnets exhibit great potential for advanced magnetic applications, but their practical implementation faces significant challenges rooted in intrinsic metastability and structural controllability. The metastable nature of the $ThMn_{12}$-type phase fundamentally disrupts crystallization kinetics during synthesis, while the inherently small single-domain grain size imposes additional constraints on microstructure engineering.[16,17] Generally, these intrinsic characteristics create dual obstacles: they not only impede the attainment of required phase purity but also promote unintentional coexistence of hard and soft magnetic phases — a critical issue when pursuing nanocrystallization strategies to enhance magnetic performance.[18–20]

In conventional permanent magnets, nanocrystallization enhances functional properties through two well-established mechanisms: (i) domain wall pinning at refined grain boundaries for increased high coercivity (H_c),[21–23] and (ii) directional magnetization reversal governed by grain size disparity for higher energy density.[24] However, in $ThMn_{12}$-type systems, unpredictable phase transitions during processing lead to erratic grain growth dynamics, making it exceptionally difficult to achieve both narrow size distributions and

†Corresponding author. E-mail: qianhuidong@pku.edu.cn

‡Corresponding author. E-mail: xgchen@ahu.edu.cn

§Corresponding author. E-mail: jbyang@pku.edu.cn

© 2025 Chinese Physical Society and IOP Publishing Ltd. All rights, including for text and data mining, AI training, and similar technologies, are reserved.

spatially ordered magnetic domains.[17,25] Unlike stable magnetic compounds where thermal treatments can systematically tune nanostructures, the transient crystallization pathways in $ThMn_{12}$-type materials often result in disordered domain configurations that negate the theoretical benefits of nanocrystallization.

This contradiction arises from competing requirements: the thermodynamic instability demanding rapid solidification to preserve the desired phase, versus the kinetic necessity for controlled crystallization to establish ordered nanostructures.[26–30] Consequently, achieving stable and high-performance magnets has been a significant challenge in previous research efforts.

Several approaches have been explored to address these issues, including compositional modifications and the introduction of doping elements to stabilize the $ThMn_{12}$-type phase. Most studies tend to increase the stability of the $ThMn_{12}$-type structure by adding stability-enhancing elements; however, this often results in a significant decrease in magnetization, as observed with the substitution of Fe by Ti, V, Cr, Mn, Mo, W, Si, and Al.[31–42]

Few reports reveal that B can form B-rich boundary phases at the grain boundaries of $ThMn_{12}$-type films, which serve to magnetically isolate the grains.[43,44] In the context of ribbons, B appears to induce the precipitation of Ti-rich phases or grain refinement, thereby enhancing the magnetic performance of the samples.[45,46] This suggests that B has a significant effect on the modification of grain boundaries, which is closely related to the H_c of $ThMn_{12}$-type magnets. However, whether B plays additional roles in $ThMn_{12}$-type magnets remains unclear, presenting considerable research value for further exploration.

Furthermore, relatively little research has focused on the control of $ThMn_{12}$-type magnets' microstructure and the simplification of the overall fabrication process. In traditional methodologies, the preparation of nano/microcrystalline magnets typically follows one of two approaches: the first involves melting, homogenization, and refinement;[47] the second involves melting, amorphization, and grain growth.[48] The distinction lies in whether nano/microcrystals are formed directly or whether existing large particles are refined to produce nano/microcrystalline magnets or magnetic powders. However, the complex preparation steps hinder potential industrial-scale production of the metastable $ThMn_{12}$-type magnets. Therefore, simplifying the fabrication process and addressing the metastable characteristics of $ThMn_{12}$-type magnets are the critical factors in developing this magnet, which is valuable for both scientific research and industrial application.

In this study, $ThMn_{12}$-type $Sm_{0.8}Zr_{0.2}Fe_{11}SiB_x$ ($x = 0$–0.2) ribbon magnets were successfully synthesized through a one-step rapid solidification process. The introduction of B into the alloy composition significantly enhanced the phase stability of the $ThMn_{12}$-type structure, enabling the direct formation of a high-purity phase. Furthermore, by carefully optimizing the B concentration and cooling rate, we achieved a uniform microstructure along with improved magnetic properties, including a H_c of 6222 Oe, a remanence (M_r) of 80 emu/g, and a remanence ratio (M_r/M_s) of 0.71. These findings highlight the effectiveness of B doping and one-step processing in addressing the challenges of phase instability and complex preparation requirements, offering a promising strategy for the scalable production of $ThMn_{12}$-type magnets with high performance and simplified fabrication processes.

2. Experiment

Ingots with nominal compositions, $Sm_{0.8}Zr_{0.2}Fe_{11}SiB_x$ ($x = 0$–0.2), were prepared by arc-melting high-purity Sm (99.9%), Zr (99.9%), Fe (99.9%), Si (99.9%), and Fe–B (weight fraction ratio of 8:2, 99%) pieces under an Ar atmosphere (99.999%). An excess of Sm of 30 at.% was included in the alloys to compensate for Sm evaporation loss and obtain a high-purity $ThMn_{12}$-type phase. The ingots were melted in an Ar environment in quartz nozzles and ejected through a 0.4 mm orifice using pressurized Ar gas (99.999%) onto a copper wheel rotating at 20–35 m/s.

The crystal structure and phase purity of the resulting products were examined by x-ray diffraction (XRD) with Cu $K\alpha$ radiation ($\lambda = 1.5406$ Å). The cross-sectional morphologies of the bulk samples were scrutinized with a field emission scanning electron microscope (FE-SEM). The magnetic characteristics of the samples were measured with a physical property measurement system (PPMS) from Lakeshore.

3. Results and discussion

Figure 1 presents the XRD results of three samples with varying B contents after ribbon casting at different wheel speeds. As shown, an increase in wheel speed accelerates the cooling rate from the molten state, and amorphization was more severe, with the sample at 35 m/s effectively transitioning to an amorphous state. This behavior aligns with the typical characteristics of $ThMn_{12}$-type ribbons during rapid solidification.

When comparing the three samples with different B contents at the same wheel speed, it is evident that increasing B content leads to notable differences in phase formation. Overall, higher B concentrations facilitate the transition of samples to an amorphous state or result in finer grain sizes under identical rapid solidification conditions. This effect can be attributed to B acting as an amorphizing agent, which effectively suppresses grain growth during the rapid solidification process. This characteristic underpins our decision to utilize B to induce the formation of $ThMn_{12}$-type grains.

From Fig. 1, it is evident that at a wheel speed of 20 m/s, the B_0 and $B_{0.1}$ samples primarily form the $TbCu_7$-type phase, with a small amount of α-Fe phase observed in the B_0 sample. When the wheel speed increases to 30 m/s, clear diffraction peaks appear at 42.222°, 42.481°, and 43.249°, which indicates the appearance of $ThMn_{12}$-type $Sm_{0.8}Zr_{0.2}Fe_{11}SiB_x$. As the wheel speed further increases to 35 m/s, the B_0 sample exhibits a mixture of amorphous and $ThMn_{12}$-type phases, while the $B_{0.1}$ sample is almost entirely amorphous. For the $B_{0.2}$ sample, a clear presence of a mixed phase of amorphous and $ThMn_{12}$-type phases is evident at 20 m/s, and complete amorphization occurs at both 30 m/s and 35 m/s.

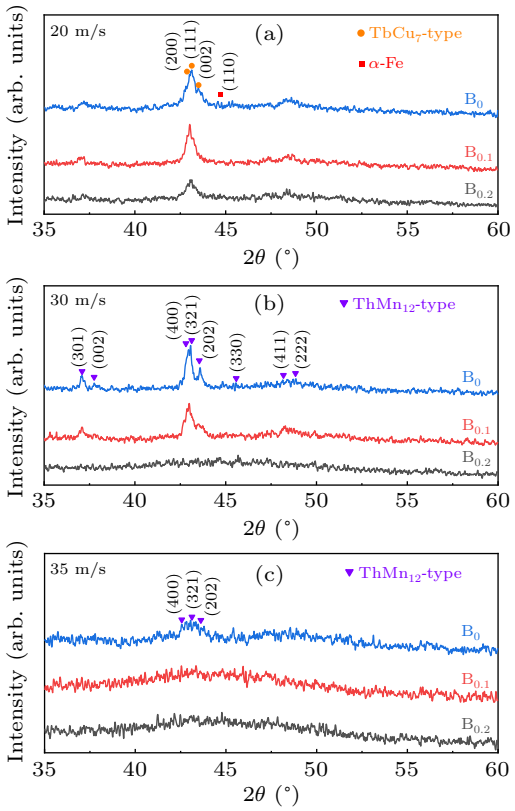


Fig. 1. XRD patterns of rapidly solidified $Sm_{0.8}Zr_{0.2}Fe_{11}SiB_x$ ($x = 0$–0.2) ribbons with Cu wheel speeds of (a) 20 m/s, (b) 30 m/s, and (c) 35 m/s.

These observations suggest that the addition of trace amounts of B effectively inhibits the crystallization of the $ThMn_{12}$-type phase during rapid solidification. Such suppression is beneficial for achieving nanocrystalline $ThMn_{12}$-type grains while avoiding the formation of significant amounts of α-Fe soft magnetic phase, thereby ensuring the purity of the $ThMn_{12}$-type phase within the samples.

Figure 2 presents the magnetic performance testing results of samples with three different B contents, cast at varying wheel speeds. The data indicate that the magnetic properties are optimal at a wheel speed of 30 m/s. This can be attributed to two factors: first, the samples prepared at 20 m/s contain a significant amount of the $TbCu_7$-type phase and a small amount of α-Fe phase; second, the samples cast at 30 m/s likely have a more suitable grain size compared to those produced at 20 m/s. Conversely, at a wheel speed of 35 m/s, many samples exhibit signs of amorphization, leading to a decline in magnetic performance. Therefore, our discussion primarily focuses on the magnetic properties and microstructure of the samples prepared at 30 m/s. Respectively, the H_c values for the B_0 and $B_{0.1}$ samples reached 3912 Oe and 6222 Oe at a wheel speed of 30 m/s. The introduction of trace amounts of B significantly enhances the H_c, yielding an increase of approximately 59%. Due to trace element doping, such a substantial increase in H_c is relatively rare; most studies on $ThMn_{12}$-type materials have primarily adjusted H_c through significant changes in grain size and alloy composition.

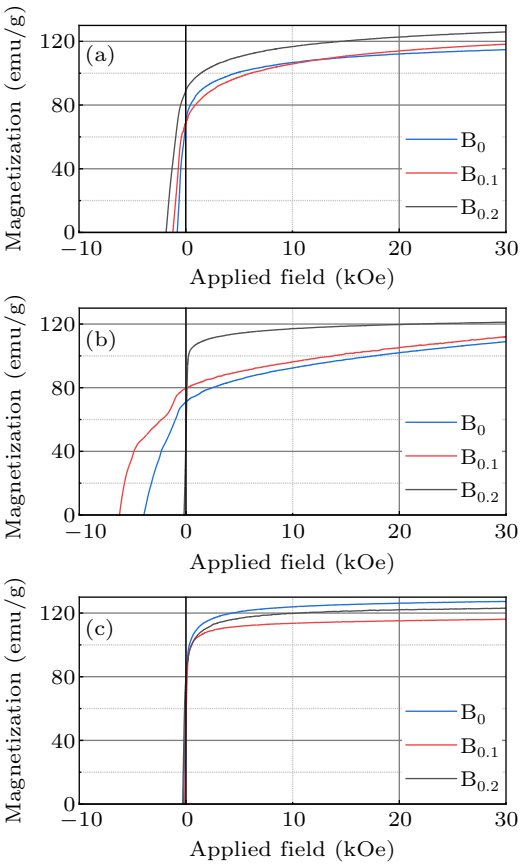


Fig. 2. Magnetic hysteresis loops of rapidly solidified $Sm_{0.8}Zr_{0.2}Fe_{11}SiB_x$ ($x = 0$–0.2) ribbons with Cu wheel speeds of (a) 20 m/s, (b) 30 m/s, and (c) 35 m/s.

Table 1. Magnetic properties of rapidly solidified $Sm_{0.8}Zr_{0.2}Fe_{11}SiB_x$ ($x = 0$–0.2) ribbons with different Cu wheel speeds.

x	v (m/s)	H_c (Oe)	M_r (emu/g)	M_s (emu/g)	M_r/M_s
0	20	794	69	115	0.60
0.1	20	1199	69	118	0.58
0.2	20	1837	88	126	0.70
0	30	3912	71	109	0.65
0.1	30	6222	80	112	0.71
0.2	30	181	50	121	0.41
0	35	221	73	127	0.57
0.1	35	111	52	116	0.44
0.2	35	312	79	123	0.64

The XRD results confirm that trace B doping has a pronounced effect on inhibiting grain growth, suggesting that B plays a crucial role in optimizing H_c. However, aside from inhibiting grain growth, it remains unclear whether other effects are present that may influence magnetic properties, particularly regarding the sample's crystal structure and microstructure. Therefore, further investigation is warranted to elucidate the additional impacts of B on the magnetic performance of the samples, as this may reveal further avenues for optimizing magnetic properties.

Figure 3 presents the magnetization versus temperature (MT) curves of the B_0, $B_{0.1}$, and $B_{0.2}$ samples prepared at a wheel speed of 30 m/s. The XRD patterns from Fig. 1 indicate that the peak intensities of the nanocrystalline/amorphous samples are insufficient to accurately determine whether B directly affects the crystal structure of the $ThMn_{12}$-type phase. Therefore, MT measurements were conducted to assess whether the Curie temperature (T_c) varies significantly with the addition of B.

The results indicate that the T_c of the B_0 and $B_{0.1}$ samples are relatively similar, suggesting that their crystal structures do not exhibit significant changes. However, the MT curve for the B_0 sample shows some optimization, which may be attributed to its lower purity compared to the $B_{0.1}$ sample, resulting in the presence of minor secondary phases. The reduction of these secondary phases could be one of the factors contributing to the optimization of the magnetic properties.

In contrast, the T_c of the $B_{0.2}$ sample is significantly lower than that of the B_0 and $B_{0.1}$ samples. This can be attributed to the fact that the $B_{0.2}$ sample is nearly entirely amorphous, and the T_c of amorphous samples typically differs considerably from that of $ThMn_{12}$-type materials. This observation reinforces the notion that the structural characteristics of the samples play a crucial role in determining their magnetic behavior. Further investigation into the relationship between the amorphous nature and magnetic properties of the $B_{0.2}$ sample is warranted to fully understand these dynamics.

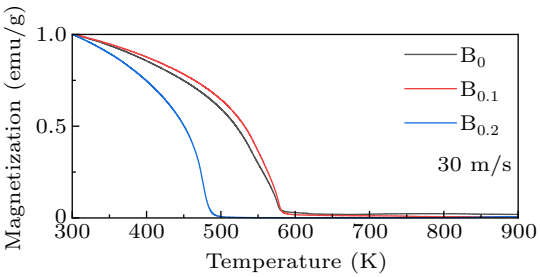


Fig. 3. MT curves (200 Oe) of the $Sm_{0.8}Zr_{0.2}Fe_{11}SiB_x$ ($x = 0$–0.2) ribbons prepared at a wheel speed of 30 m/s.

Figure 4 presents FE-SEM images for the B_0, $B_{0.1}$, and $B_{0.2}$ samples prepared at a wheel speed of 30 m/s. As confirmed in Fig. 3, trace amounts of B do not appear to have a significant effect on the $ThMn_{12}$-type crystal structure, suggesting that the changes in H_c are not attributable to alterations in crystal structure. Consequently, FE-SEM analysis was conducted to investigate whether the microstructural characteristics of the samples had undergone changes.

Table 2. The T_c of $Sm_{0.8}Zr_{0.2}Fe_{11}SiB_x$ ($x = 0$–0.2) ribbons prepared at a wheel speed of 30 m/s.

x	T_c (K)
0	579
0.1	582
0.2	488

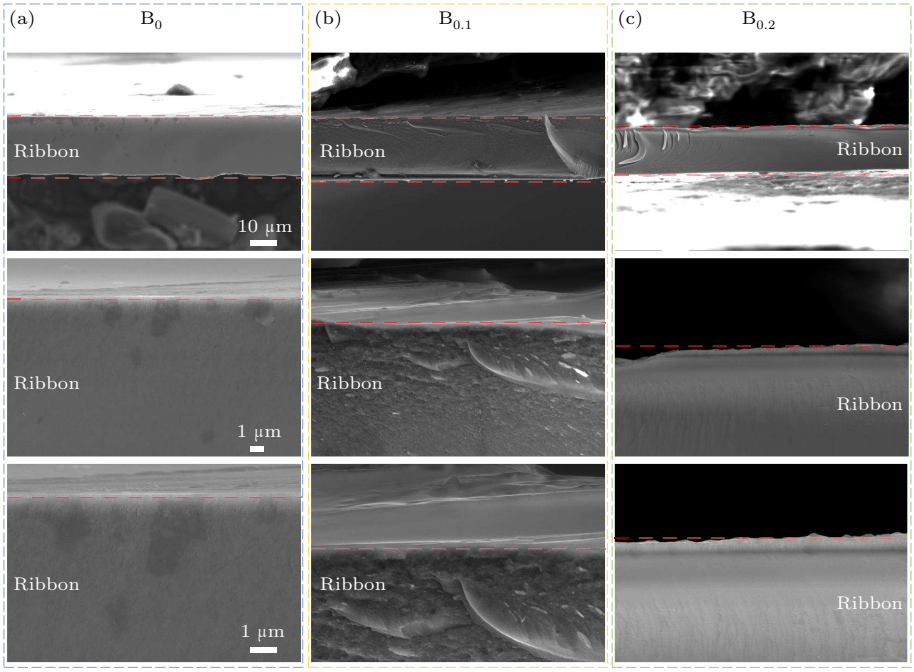


Fig. 4. Cross section FE-SEM images of $Sm_0.8Zr_0.2Fe_{11}SiB_x$ ($x = 0$–0.2) ribbons with B content of (a) 0, (b) 0.1, and (c) 0.2 prepared at a wheel speed of 30 m/s.

The images were taken from the vertical cross-sections of the ribbon samples, which were freshly exposed by breaking the ribbons rather than by polishing. Polishing was avoided due to the excessively fine grain sizes, which would obscure useful information. At low magnifications, the FE-SEM images reveal significant differences in the cross-sectional structures of the three samples, with the only variable being the trace B doping. The B_0 sample exhibits a generally uniform and smooth morphology; however, certain regions display pronounced differences in brightness, indicating compositional variations. This segregation is attributed to the metastable characteristics of the $ThMn_{12}$-type structure during the rapid solidification process, which affects the final consistency of the samples and consequently influences their magnetic properties.

In contrast, the $B_{0.1}$ sample shows substantial changes in microstructure. Upon magnification of specific regions, a uniformly fine-grained structure becomes apparent. These structures are likely formed during fracture, indicating multiple fine interface layers. During the fracture process, the differing stress distributions within these layers and the grain interiors produce a serrated morphology. The abundance of interfaces may contribute to the significant increase in H_c observed in the $B_{0.1}$ sample, as these interfaces can act as pinning sites during magnetization reversal, impeding the process and thereby enhancing H_c.

When the B content is increased to 0.2, the distinctive fine-grained structure disappears, leaving only smaller grain features that are barely discernible. Comparison with the XRD results indicates that the $B_{0.2}$ sample has nearly transformed into an amorphous state during rapid solidification, making it challenging to identify any distinct fine-grained or interface morphology in the cross-section. This observation underscores the impact of B doping on the microstructural evolution and magnetic properties of $ThMn_{12}$-type magnets.

4. Conclusion

This work primarily investigates the changes in magnetic properties of $ThMn_{12}$-type ribbon samples with the alloy composition $Sm_{0.8}Zr_{0.2}Fe_{11}SiB_x$ ($x = 0$–0.2) under varying cooling rates (wheel speeds of 20–35 m/s) and different B contents. The sample $Sm_{0.8}Zr_{0.2}Fe_{11}SiB_x$, subjected to rapid solidification at a wheel speed of 30 m/s, successfully achieves H_c, M_r, and M_r/M_s values of 6222 Oe, 80 emu/g, and 0.71, respectively. This study identifies and explores the effects of B on inhibiting grain growth of the $ThMn_{12}$-type phase, its role in suppressing segregation during rapid solidification, and its impact on optimizing microstructure. The findings suggest that trace amounts of B can significantly enhance the magnetic performance of $ThMn_{12}$-type magnets produced via rapid solidification, and indicate potential unknown effects that warrant further investigation.

Acknowledgments

Project supported by the National Key R&D Program of China (Grant Nos. 2021YFB3500300 and 2023YFB3507000) and the Scientific Research Foundation of the High Education Institutions for Distinguished Young Scholars in Anhui Province (Grant No. 2022AH020012). This work was also partially supported by the Innovation Project for Overseas Researcher in Anhui Province (Grant No. 2022LCX004) and the facilities at the Center of Free Electron Laser & High Magnetic Field (FEL&HMF) in Anhui University.

References

[1] Chau K T, Chan C C and Liu C 2008 *IEEE Trans. Ind. Electron.* **55** 2246
[2] Chinchilla M, Arnaltes S and Burgos J C 2006 *IEEE Trans. Energy Convers.* **21** 130
[3] Pullar R C 2012 *Prog. Mater. Sci.* **57** 1191
[4] Hadjipanayis G C, Gabay A M, Schönhöbel A M, Martín-Cid A, Barandiaran J M and Niarchos D 2020 *Engineering* **6** 141
[5] Qian H, Wang F, Liang D, Lin Z, Han J and Yang J 2023 *J. Chin. Soc. Rare Earths* **41** 439
[6] Herbst J F 1991 *Rev. Mod. Phys.* **63** 819
[7] Coey J M D 2020 *Engineering* **6** 119
[8] Yang Y X, Walton A, Sheridan R, Güth K, Gauss R, Gutfleisch O, Buchert M, Steenari B M, Van Gerven T, Jones P T and Binnemans K 2017 *J. Sustain. Metall.* **3** 122
[9] Buschow K H J 1991 *Rep. Prog. Phys.* **54** 1123
[10] Takahashi Y K, Sepehri-Amin H and Ohkubo T 2021 *Sci. Technol. Adv. Mater.* **22** 449
[11] Bessais L 2022 *Materials* **15** 201
[12] Hirayama Y, Takahashi Y K, Hirosawa S and Hono K 2017 *Scr. Mater.* **138** 62
[13] Yang Y C, Zhang X D, Ge S L, Pan Q, Kong L S, Li H, Yang J L, Zhang B S, Ding Y F and Ye C T 1991 *J. Appl. Phys.* **70** 6001
[14] Gabay A M and Hadjipanayis G C 2016 *J. Alloys Compd.* **657** 133
[15] Gabay A M, Martín-Cid A, Barandiaran J M, Salazar D and Hadjipanayis G C 2016 *AIP Adv.* **6** 056015
[16] Xiao Q F, Zhang Z D, Zhao T, Liu W, Sui Y C, Zhao X G and Geng D Y 1997 *J. Appl. Phys.* **82** 6170
[17] Khazzan S, Bessais L, Van Tendeloo G and Mliki N 2014 *J. Magn. Magn. Mater.* **363** 125
[18] Li X H, Lou L, Song W P, Huang G W, Hou F C, Zhang Q, Zhang H T, Xiao J W, Wen B and Zhang X Y 2017 *Adv. Mater.* **29** 1606430
[19] Xu D S, Liu L, Yuan J H, Zhou B, Dong C H, Wang F Q, Ding Y, Sun Y L and Yan A R 2024 *Chin. Phys. B* **33** 098103
[20] Ener S, Skokov K P, Palanisamy D, Devillers T, Fischbacher J, Eslava G G, Maccari F, Schäfer L, Diop L V B, Radulov I, Gault B, Hrkac G, Dempsey N M, Schrefl T, Raabe D and Gutfleisch O 2021 *Acta Mater.* **214** 116968
[21] Hua Y X, Li X H, Li J X, Luo X, Li Y Q, Qin W Y, Zhang L Q, Xiao J W, Xia W X, Song P, Yue M, Zhang H T and Zhang X Y 2024 *Science* **385** 634
[22] Schrefl T, Fidler J and Kronmüller H 1994 *Phys. Rev. B* **49** 6100
[23] Hadjipanayis G C 1999 *J. Magn. Magn. Mater.* **200** 373
[24] Lou L, Li Y Q, Li X H, Li H L, Li W, Hua Y X, Xia W X, Zhao Z H, Zhang H T, Yue M and Zhang X Y 2021 *Adv. Mater.* **33** 2102800
[25] Schönhöbel A M, Madugundo R, Barandiaran J M, Hadjipanayis G C, Palanisamy D, Schwarz T, Gault B, Raabe D, Skokov K, Gutfleisch O, Fischbacher J and Schrefl T 2020 *Acta Mater.* **200** 652
[26] Zhang H T and Zhang X Y 2022 *Mater. Res. Lett.* **10** 1

[27] Li X H, Lou L, Li Y Q, Zhang G S, Hua Y X, Li W, Zhang H T, Yue M and Zhang X Y 2022 *Nano Lett.* **22** 7644

[28] Zhang X Y, Hua Y X and Li X H 2025 *Sci. China Phys. Mech. Astron.* **68** 247511

[29] Zhang H T, Zhang T and Zhang X Y 2023 *Adv. Sci.* **10** 2300193

[30] Lou L, Li J X, Luo X, Zhang T, Li X Z, Zhu Q Y, Du Y, Bi Z W, Sun X H, Cheng Q W, Xiao Y T, Zhao S T, Wen B, Zhang X Y and Zhang H T 2025 *Nat. Commun.* **16** 3094

[31] Zhang X F, Liu L B, Li Y Q, Zhang D T, Liu W Q and Yue M 2024 *Chin. Phys. B* **33** 097503

[32] Wang C Z, Liu L, Sun Y L, Zhao J T, Zhou B, Tu S S, Wang G C, Ding Y and Yan A R 2023 *Chin. Phys. B* **32** 020704

[33] Qian H D, Lim J T, Kim J W, Yang Y, Zhou T H, Jeon H K, Park J and Choi C J 2022 *Metals* **12** 753

[34] Buschow K H J 1991 *J. Magn. Magn. Mater.* **100** 79

[35] Tozman P, Sepehri-Amin H, Takahashi Y K, Hirosawa S and Hono K 2018 *Acta Mater.* **153** 354

[36] Srinithi A K, Tang X, Sepehri-Amin H, Zhang J, Ohkubo T and Hono K 2023 *Acta Mater.* **256** 119111

[37] Tang X, Li J, Srinithi A K, Sepehri-Amin H, Ohkubo T and Hono K 2021 *Scr. Mater.* **200** 113925

[38] Yang J B, Mao W H, Yang Y C, Ge S L, Zhao Z J and Li F S 1998 *J. Appl. Phys.* **83** 2700

[39] Lin Z, Han J Z, Liu S Q, Xing M Y, Yang Y B, Yang J B, Wang C S, Du H L and Yang Y C 2012 *J. Magn. Magn. Mater.* **324** 196

[40] Fan S H, Wu B C, Qian H D, Xia Y H, Li H, Chen G X, Xu Q, Yang W Y, Han J Z, Du H L, Yang J B and Yang Y C 2024 *Mater. Today Phys.* **41** 101348

[41] Fan S H, Wang F G, Xia Y H, Wu B C, Qian H D, Lin Z C, Wang Y K, Du H L, Yang J B and Yang Y C 2023 *Mater. Today Phys.* **35** 101119

[42] Zhou T H, Qian H D, Lim J T, Jeon H K, Choi C J, Cho Y R and Park J 2023 *J. Alloys Compd.* **966** 171620

[43] Sepehri-Amin H, Tamazawa Y, Kambayashi M, Saito G, Takahashi Y K, Ogawa D, Ohkubo T, Hirosawa S, Doi M, Shima T and Hono K 2020 *Acta Mater.* **194** 337

[44] Bolyachkin A, Sepehri-Amin H, Kambayashi M, Mori Y, Ohkubo T, Takahashi Y K, Shima T and Hono K 2022 *Acta Mater.* **227** 117716

[45] Liu Z Y, Liu Z, Wu H C, Zhu C Q, Cheng W X, Cao S, Luo H B, Wu L, Chen R J, Xia W X, Feng H B and Yan A R 2023 *Scr. Mater.* **227** 115281

[46] Gabay A M and Hadjipanayis G C 2021 *J. Magn. Magn. Mater.* **529** 167867

[47] Zhang J S, Tang X, Bolyachkin A, Srinithi A K, Ohkubo T, Sepehri-Amin H and Hono K 2022 *Acta Mater.* **238** 118228

[48] Qian H D, Lim J T, Kim J W, Yang Y, Cho K M, Park J and Choi C J 2021 *Scr. Mater.* **193** 17